Journal of Rare Earths 39 (2021) 1382–1388

Contents lists available at ScienceDirect

Journal of Rare Earths

journal homepage: http://www.journals.elsevier.com/journal-of-rare-earths

# An egg-shell bifunctional $CeO_2$-modified $NiPd/Al_2O_3$ catalyst for petrochemical processes involving selective hydrogenation and hydroisomerization☆

Franklin J. Méndez [a, b, *], Javier A. Alves [c], Yahsé Rojas-Challa [d], Oscar Corona [e, f], Yanet Villasana [a, g], Julia Guerra [h], Germán García-Colli [c], Osvaldo M. Martínez [c], Joaquín L. Brito [a]

[a] Centro de Química, Instituto Venezolano de Investigaciones Científicas, Carretera Panamericana, Km 11 Altos de Pipe, Caracas, 1020A, Venezuela
[b] Departamento de Estado Sólido, Instituto de Física, Universidad Nacional Autónoma de México, Ciudad Universitaria, Ciudad de México, 04510, México
[c] Departamento de Ingeniería Química, Facultad de Ingeniería (UNLP) and Centro de Investigación y Desarrollo en Ciencias Aplicadas "Dr. J.J. Ronco" (CINDECA) CCT-La Plata-CONICET-UNLP, La Plata, 1900, Argentina
[d] Departamento de Química Analítica, Facultad de Química, Universidad Nacional Autónoma de México, Ciudad Universitaria, Ciudad de México, 04510, México
[e] Instituto Tecnológico Venezolano Del Petróleo S.A., Petróleos de Venezuela S.A., Urb. Santa Rosa-Sector El Tambor, Los Teques, 1201, Venezuela
[f] Instituto Superior de Formación Docente Salomé Ureña, Esquina Leonardo D'Vinci, Santo Domingo, 10114, República Dominicana
[g] Biomass to Resources Group, Universidad Regional Amazonica Ikiam, Km 7 vía Muyuna, Tena, 150150, Ecuador
[h] Departamento de Termodinámica y Fenómenos de Transferencia, Universidad Simón Bolívar, Valle de Sartenejas, Caracas, 1086, Venezuela

ARTICLE INFO

*Article history:*
Received 21 June 2020
Received in revised form
11 September 2020
Accepted 24 September 2020
Available online 6 October 2020

*Keywords:*
1-Butyne
Bifunctional catalyst
Egg-shell
Hydrogenation
Hydroisomerization
NiPd catalyst

ABSTRACT

The catalytic performance during the 1-butyne hydrogenation using two reduced $Al_2O_3$-supported Pd-based catalysts was carried out in a total recirculation system with an external fixed-bed reactor. The lab-prepared egg-shell $NiPd/CeO_2$-$Al_2O_3$ catalyst (NiPdCe) with Pd loading = 0.5 wt%, Ni/Pd atomic ratio = 1 and $CeO_2$ loading = 3 wt% was synthesized and characterized, and it was compared with an egg-shell $Al_2O_3$-supported Pd based commercial catalyst (PdCC). The reduced catalysts were characterized by X-ray diffraction, X-ray photoelectron spectroscopy, and high-resolution transmission electron microscopy. The textural characteristics and ammonia temperature-programmed desorption profiles of the fresh (unreduced) catalysts were also obtained. Both catalysts show high 1-butyne conversion and selectivity to 1-butene, but the catalysts also present important differences between hydroisomerizing and hydrogenating capabilities. NiPdCe catalyst shows higher capability for hydroisomerization reactions, while the PdCC catalyst exhibits higher hydrogenating capability. The observed catalytic performances can be interesting for some industrial processes and can provide a guideline for the development of a Pd-based catalyst with specific catalytic properties.



## 1. Introduction

Most petrochemical industries include hydrorefining reactors for the upgrading of C4 cuts originated during cracking operations, in which 1,3-butadiene, 1-butyne, iso-butene, 1-butene, and 2-butenes are simultaneously produced.[1] To take advantage of these cuts as industrial streams, several hydrorefining operations have been developed, in which hydroalkylation and hydrogenation reactions have attracted attention for decades, where the transformation of traces of unsaturated compounds, such as 1,3-butadiene and 1-butyne, is the most important challenge[2] because these reactions proceed under strong diffusion

☆ **Foundation item:** Project supported by the Fondo Nacional de Ciencia, Tecnología e Innovación (FONACIT-G-2005000437), Universidad Nacional de La Plata (UNLP-PID I226), Consejo Nacional de Investigaciones Científicas y Técnicas (CONICET-PIP 0018) and Agencia Nacional de Promoción Científica y Tecnológica (ANPCyT-PICT 2015/3546).

* Corresponding author. Departamento de Estado Sólido, Instituto de Física, Universidad Nacional Autónoma de México, Ciudad Universitaria, Ciudad de México, 04510, México.
*E-mail addresses:* fmendez@fisica.unam.mx, frankmendez.mz@gmail.com (F.J. Méndez).

https://doi.org/10.1016/j.jre.2020.09.017

limitations, causing significant losses of the desired-product.[3–6] Thus, the selectivity toward the formation of the desired product and hydroisomerization/hydroisomerization capabilities should be the most important parameters in these petrochemical processes along with the requirements of high activity and stability.[5]

Current technologies use catalytic fixed-bed reactors with the concurrent flow of the liquid hydrocarbons and gaseous hydrogen. The operating temperatures ranging from room temperature up to around 60–70 °C and total pressure from atmospheric up to about 1400 kPa are used to maintain the hydrocarbon stream in the liquid-phase, allowing the desired level of hydrogen partial pressure.[2,6] The resulting hydrogen partial pressure in the gas phase and its corresponding molar fraction in the liquid phase are about 500 kPa and 0.5 mol%, respectively.

Some noble metals, such as Rh, Ru, Pd, and Pt, have been used for a long time as the active component for hydroisomerization and selective hydrogenation reactions.[7] However, $Al_2O_3$-supported Pd-based catalysts (0.05 wt% to 0.5 wt% metal content) have been shown as the most active and selective catalyst in both petrochemical processes due to the stronger adsorption of 1-butyne (or 1,3-butadiene) on the metal surface as compared with the desired product, 1-butene. To minimize contact time of the active sites and reactants/products, a vital characteristic of such catalysts is that the active phase is distributed as egg-shell.[8] Previous studies have demonstrated that Pd particle size, support acidity and the presence of other transition metals have a significant influence on the activity and selectivity for several petrochemical applications.

Pd in combination with a second metal such as Cu, Ag, Au, has also been used as catalytic systems to improve the performance.[9] The use of Ni as second metal in Pd egg-shell catalysts is comparatively much less reported than other bimetallic combinations.[10–15] On the other hand, ceria has many interesting applications[16] but, to the best of our knowledge, has not been employed to modify the characteristics of the supports for selective hydrogenation and hydroisomerization.[17–19] Our lab has involved in research of new $Al_2O_3$-supported NiPdCe-based formulations for several years.[17–20] It has been demonstrated that Ni- and Ce-incorporation to the Pd/$Al_2O_3$ catalyst, and toluene-addition to the reaction feed, affect the metals dispersion and diolefin adsorption. Furthermore, both activity and selectivity have been improved during the selective hydrogenation of 1,3-butadiene in the presence of 1-butene. 1-Butyne is another important pollutant in the C4 cuts which requires attention, while the hydroisomerization function of our NiPdCe catalyst, and its relationship with hydrogenation remain unexplored and could be important for future industrial applications. On the other hand, the comparison between synthesized-model with current industrial catalysts (typically subjected to confidentiality agreements) is scarce, if at all published. In the present study, we examined the catalytic parameters of an egg-shell bifunctional NiPd/$CeO_2$-$Al_2O_3$ catalyst and compared it with a promoted Pd/$Al_2O_3$ commercial catalyst under conditions that allow the best catalytic behaviour during the reaction.

## 2. Experimental

### 2.1. Catalyst preparation

The metal incorporations were carried out by wet impregnation from aqueous solutions, using ammonium cerium (IV) nitrate (Alfa Aesar), nickel(II) nitrate hexahydrate (Sigma-Aldrich) and tetraamminepalladium (II) chloride monohydrate (Sigma-Aldrich) as precursors. The experimental details are described in the Electronic Supplementary Information, ESI. The NiPd/$CeO_2$-$Al_2O_3$ catalyst (denoted as NiPdCe) showed a Pd loading of 0.5 wt%, Ni/Pd atomic ratio equal to 1 and $CeO_2$ amount of 3 wt% and the obtained cylindrical pellets presented an external layer containing $CeO_2$-$Al_2O_3$-supported NiPd particles (~150 μm in depth) and a core with only $CeO_2$ and $Al_2O_3$. Some additional characterization results of metal content, including elemental mapping along the pellets cross-section, can be seen in our previous article.[19]

### 2.2. Commercial catalyst

An egg-shell Pd-based commercial catalyst (denoted as PdCC) supported on spherical $Al_2O_3$ was also used. The manufacturer's information mentioned that this catalyst presents a mean diameter of 2.34 mm and 230 μm external layer of $Al_2O_3$-supported Pd particles and an $Al_2O_3$ inert core. Furthermore, it is also declared that the catalyst was modified but the promotor(s) characteristics are not mentioned, such as metal type or amount.

### 2.3. Physicochemical characterization

Powder XRD patterns were obtained between $2\theta$ range of 20° and 80° with a SIEMENS D-5005 diffractometer using Cu Kα radiation. Nitrogen physisorption data were obtained with a MICROMERITICS ASAP 2010 automatic analyser at liquid $N_2$ temperature. HRTEM micrographs were obtained with a JEOL JEM-2100 microscope with $LaB_6$ filament operating at 200 kV. XPS spectra were obtained using a SPECS PHOIBOS 150 spectrometer equipped with a LEYBOLD vacuum system operating at $1.33 \times 10^{-6}$ Pa and Al Kα ($E = 1486.6$ eV) as the radiation source. $NH_3$-TPD thermograms were obtained from 40 to 500 °C using a MICROMERITICS AUTOCHEM II 2920 automatic analyser.

### 2.4. Catalytic test

#### 2.4.1. Reduction treatment

The unmilled NiPdCe catalyst was loaded in a stainless steel fixed-bed reactor of ¼ in internal diameter and reduced *in situ* under 30 mL/min flow of $H_2$ at 300 °C, this temperature was reached at a linear rate of 3 °C/min, which was held for 2 h. The unmilled PdCC catalyst was reduced according to the manufacturer's recommended protocol.[5]

#### 2.4.2. Liquid-phase 1-butyne hydrogenation

The reagents were purified just before tests because it is well-known that the moisture decreases the catalyst performance[5] (see their details in the Electronic Supplementary Information, ESI). Liquid-phase reactivity measurements were carried out in a total recirculating system with an external fixed-bed reactor (see ESI, Scheme S1). The recirculation at a high rate (700 mL/min) from the stirred vessel (AUTOCLAVE ENGINEERS EZE-Seal) to the external reactor and back to stirred vessel was carried out using a magnetically driven gear micropump (MICROPUMP 200). The stirred vessel allowed loading the initial hydrocarbon mixture, feeding $H_2$ continuously, and maintaining the liquid saturated with $H_2$ during the runs. All experiments were performed with 250 mg of catalyst, an initial molar composition of 1-butyne of 7.0%, a temperature of 44 °C, a total pressure of 700 kPa and agitation speed of 2000 r/min.[21]

The liquid effluent stream from the reactor was analysed with an on-line gas chromatograph (SHIMADZU model GC-8A) equipped with a flame ionization detector and a column packed with 0.19% picric acid on GRAPHPAC-GC 80/100 (ALLTECH, 213.36 cm length and 0.32 cm internal diameter). The control of the $H_2$ partial pressure during runs was tested by analysing the vapor-phase in a conductivity cell.

## 3. Results and discussion

### 3.1. Catalyst characterization

The structural identification of the different $Al_2O_3$-phases was traditionally carried out using XRD or $^{27}$Al-MAS-NMR analysis. As samples change from γ-$Al_2O_3$ → δ-$Al_2O_3$ → θ-$Al_2O_3$, the XRD patterns do not exhibit abrupt changes but show the gradual appearance of new features, related to their crystallinity.

#### 3.1.1. X-ray diffraction

XRD results of both reduced $Al_2O_3$-supported Pd-based catalysts are shown in Fig. 1. The diffractogram of the most crystalline catalyst (PdCC) presents seven signals at 32.6°(022), 36.9°(122), 39.4°(026), 45.5°(220), 46.4°(222), 60.7°(138) and 67.1°(042)/2$\theta$, while the NiPdCe catalyst shows six peaks at 28.7°(220), 37.5°(311), 39.4°(222), 46.1°(400), 60.7°(511) and 67.1°(440)/2$\theta$. The comparison with the reference patterns illustrates the dominant δ-$Al_2O_3$ (JCPDS card number 46-1131) and γ-$Al_2O_3$ (JCPDS card number 10-0425) phases for the PdCC and NiPdCe catalysts, respectively. The NiPdCe sample also presents four visible peaks at 28.5°(111), 33.1°(200), 47.5°(220) and 56.3°(311)/2$\theta$ and two weaker contributions at 76.7°(331) and 79.1°(420)/2$\theta$ assigned to the cubic $CeO_2$ structure (JCPDS card number 81-0792). The diffractograms do not show any additional signals corresponding to the Pd crystals, probably due to the small crystallite sizes or their high dispersion in the supports. These results are consistent with our previous studies.[19]

#### 3.1.2. Textural properties

$N_2$ physisorption isotherms and pore size distributions of both unreduced $Al_2O_3$-supported Pd-based catalysts are presented in Fig. 2. The corresponding textural properties are shown in Table 1. The PdCC catalyst shows the lower specific surface area ($S_{BET}$ = 67 m$^2$/g) and a Type-IV isotherm with a narrow Type-H3 hysteresis loop at high relative pressures (between 0.8 and 1), indicating a mesoporous distribution with the higher mean pore size ($D_p$ = 17 nm). Type-H3 hysteresis loop is usually found in solids consisting of aggregates or agglomerates of particles forming slit-shaped pores with nonuniform size and/or shape. On the other hand, the synthesized catalyst also shows a Type-IV isotherm, but it presents bigger nitrogen adsorption, indicating a higher specific surface area. The NiPdCe catalyst has $S_{BET}$ = 103 m$^2$/g, which is 1.5 times higher than that of the PdCC catalyst, and lower average pore size ($D_p$ = 7 nm). Unlike PdCC, NiPdCe catalyst presented a Type-H2 hysteresis loop, which is characteristic of spheroidal cavities, voids between closely packed spherical particles or ink bottle-shaped pores, indicating that these pores are more uniform than those present in the PdCC catalyst.

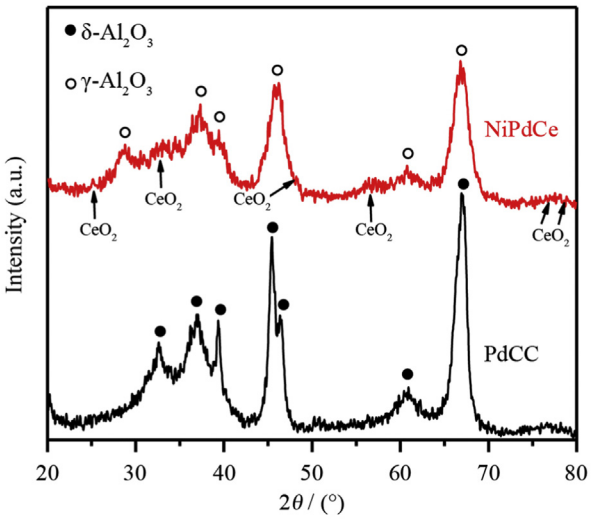


**Fig. 1.** XRD patterns of reduced $Al_2O_3$-supported Pd-based catalysts.

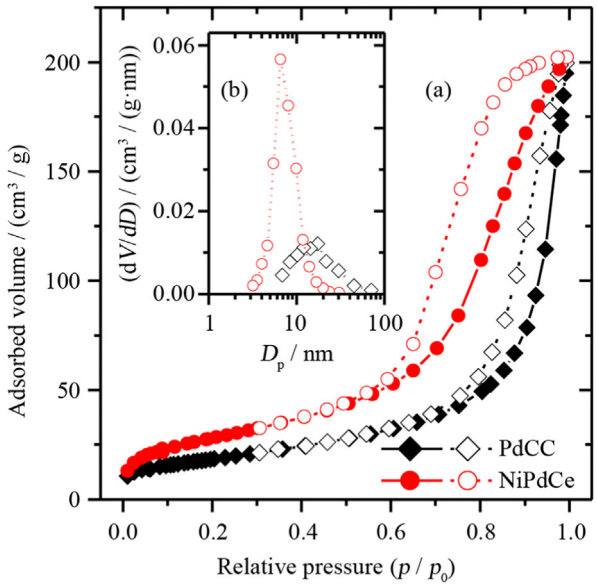


**Fig. 2.** $N_2$ physisorption isotherms (a) and pore size distributions (b) of unreduced $Al_2O_3$-supported Pd-based catalysts.

#### 3.1.3. High resolution transmission electron microscopy

HRTEM images and particle size distributions of both reduced catalysts are shown in Fig. 3. In the micrographs, many small crystallites are observed, which are visible as dark contrasts. The images also show that metal nanoparticles have uniform morphology (right side panels, Fig. 3) and they are decorating the support surface. The aggregation phenomenon is not easily visible but, other studied zones of the reduced NiPdCe catalyst (not presented here) showed aggregates containing Ni–Pd particles, which could be easily distinguished from the very small Pd particles. Some aggregates containing Ce, Pd, and Ni traces, as well as pure $CeO_2$ nanoparticles were also detected, as reported previously.[19] On the other hand, some differences can also be observed in particle size distributions (left panels, Fig. 3), as about 60% are relatively small particles for the NiPdCe catalyst with sizes nearby 1 nm, whereas the PdCC catalyst shows larger Pd particles with sizes between 2 and 3 nm. The average particle sizes are about 2.8 and 1.7 nm for the PdCC and NiPdCe catalysts, indicating that Pd particles could be better dispersed on our synthesized catalyst.

**Table 1**
Textural properties obtained by $N_2$ physisorption of unreduced $Al_2O_3$-supported Pd-based catalysts.

| Catalyst | $S_{BET}$ [a] (m$^2$/g) | $V_p$ [b] (cm$^3$/g) | $D_p$ [c] (nm) |
|---|---|---|---|
| PdCC | 67 | 0.30 | 17 |
| NiPdCe | 103 | 0.31 | 7 |

[a] Specific surface area ($S_{BET}$) was determined by the Brunauer-Emmett-Teller method.
[b] Pore volume ($V_p$) was obtained at a relative pressure close to 0.98.
[c] Mean pore diameter ($D_p$) was determined from the desorption isotherms by the Barret-Joyner-Halenda method.

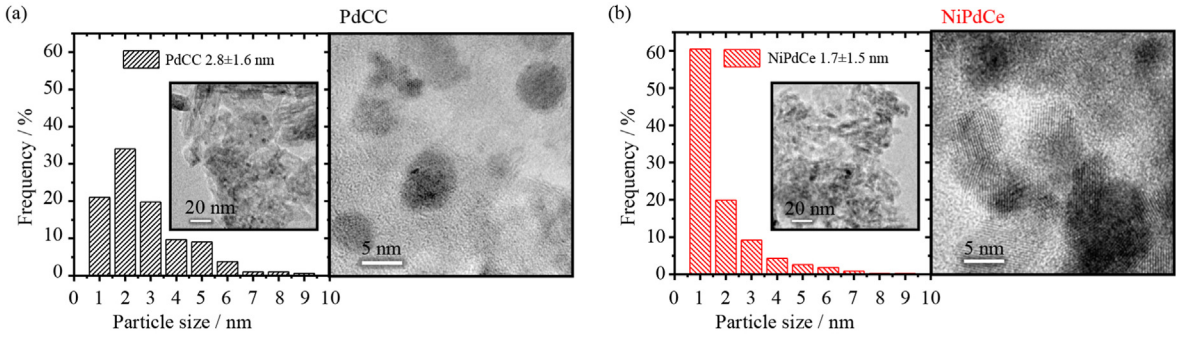


**Fig. 3.** Particle size distribution and HRTEM images of reduced $Al_2O_3$-supported Pd-based catalysts. The average particle diameter and standard deviation ($\sigma$) were calculated from $[\sum n_i d_i / \sum n_i]$ and $[\sum (d_i - d)^2 / \sum n_i]^{1/2}$, respectively, where $n_i$ is the number of particles of diameter $d_i$.

### 3.1.4. X-ray photoelectron spectroscopy

The electronic structures of both reduced $Al_2O_3$-supported Pd-based catalysts were examined by XPS. As expected, the full scan XPS spectra (ESI, Figure S1) presented both Pd 3d and Pd 3p signals. There are also peaks that were assigned to Al 2p, Al 2s, O 1s, O 2s, C 1s, and two groups of Auger lines (C KVV and O KLL). Two signals were only observed in the PdNiCe catalyst, corresponding to Ni 2p and Ce 3d regions.[22] Additional signals were expected in the PdCC catalyst but were not observed here, possibly due to the low amounts of any modifier in its formulation. The main signals (Ni 2p, Pd 3d, Ce 3d, and Al 2p) were curve-fitted (deconvoluted) and are shown in Fig. 4.

The binding energy values, at 335.6 eV (Pd $3d_{5/2}$) and 340.9 eV (Pd $3d_{3/2}$) as shown by the NiPdCe catalyst, can be assigned to the fully reduced Pd species. Both signals are slightly shifted to the lower binding energy values (~0.3 eV) when compared with the same signals for the PdCC catalyst, indicating that an interaction of metal-metal in the NiPdCe catalyst is happening (Fig. 4(b)). An additional doublet at 335.8 eV (Pd $3d_{5/2}$) and 341.1 eV (Pd $3d_{3/2}$) was observed suggesting the formation of a Ni-Pd bimetallic compound. The signals at 853.3 eV (Ni $2p_{3/2}$) and 870.2 eV (Ni $2p_{1/2}$) also correspond to an intermediate charge associated with Ni-Pd interaction (Fig. 4(a)).[23] The signal at 859.5 eV corresponds to Ni $2p_{3/2}$ satellite, while an overlap between Ni $2p_{1/2}$ satellite signal of Ni—Pd structure and Ce $3d_{5/2}$ signal cannot be discarded. The bimetallic Ni—Pd structure was previously proposed from HRTEM/STEM-HAADF results (see Ref. 19). The Ni—Pd signals (Pd 3d region) have a higher area (82.8%) than the Pd signals of the commercial catalyst (17.2%), suggesting that the NiPdCe catalyst is mainly composed of Ni-Pd nanostructures. On the other hand, it is possible that oxide species, such as a bulk oxide (PdO: Pd $3d_{5/2}$ at 337.6 eV) or intermediate oxide species ($PdO_x$: $3d_{5/2}$ at 336.4 eV), could form during the transference of samples from the reduction reactor to the UHV equipment, however, these were not observed.

The Ce 3d XPS core level spectra are shown in Fig. 4(c), in which five peaks can be identified. The signals, centered at 882.8 eV (Ce $3d_{5/2}$), 899.6 eV (Ce $3d_{3/2}$) and 917.1 eV (Ce $3d_{3/2}$), can be attributed to unreduced $Ce^{4+}$, while the peaks at 887.0 eV (Ce $3d_{5/2}$) and 904.9 eV (Ce $3d_{3/2}$) are characteristics of $Ce^{3+}$ species, suggesting the presence of a valence state mixture. The spectra of $Ce^{4+}$ and $Ce^{3+}$ oxides consist of up to ten signals overlapped to different degrees,[24,25] however, those identified here are characteristic of the two indicated species. On the other hand, it has been reported that $Ce^{3+}$ incorporation is associated with oxygen vacancies creation in the $CeO_2$ lattice as defects.[26] A signal at 531.5 eV (O 1s region) has also been associated with the oxygen vacancies[27,28] but, given the complexity of this system, it would require a very strong commitment between equipment calibration and stoichiometric oxides used as references to do exact signals assignation. The O 1s peak at 530.9 eV can be assigned to the lattice oxygen in the $CeO_2$ crystals (Fig. 4(d)), while the corresponding oxygen signal in $Ce_2O_3$ cannot be identified because of the overlap with the Al—O signal at 531.8 eV.

The superficial elemental analysis, represented as atomic ratios, obtained by the XPS technique for both reduced catalysts, is displayed in Table 2. The more crystalline phase, i.e., δ-$Al_2O_3$ in the PdCC catalyst, is expected to show lower oxygen content on the surface. Thus, the O/Al ratio is higher for the NiPdCe catalyst compared with the PdCC one. On the other hand, it can be observed that the Pd/Al ratio is higher in the NiPdCe catalyst, indicating that Pd loading is more available at the external surface to carry out the reaction. The NiPdCe catalyst shows a Ni/Pd ratio of 0.83, which is close to the nominal value (Ni/Pd = 1), however, a very low Ce/Al ratio indicates that incorporated Ce is mostly present in the core.

### 3.1.5. Ammonia temperature-programmed desorption

$NH_3$-TPD technique provides important information on the surface acidity characteristics without distinguishing between

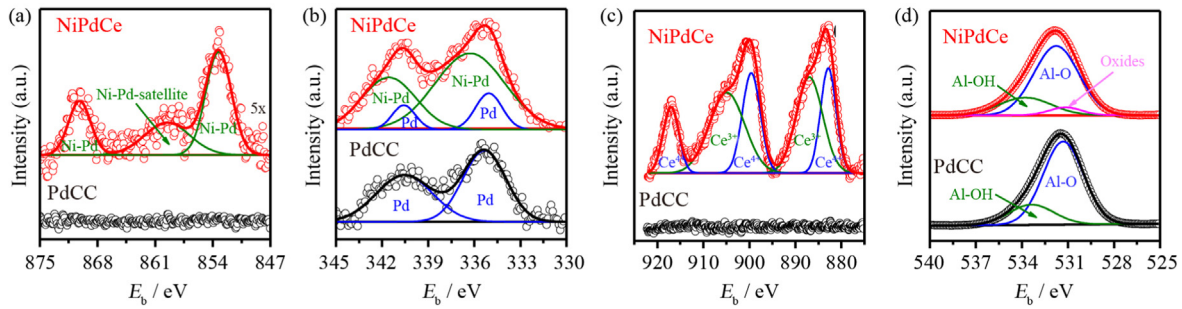


**Fig. 4.** XPS spectra of reduced $Al_2O_3$-supported Pd-based catalysts obtained at different spectral regions. (a) Ni 2p; (b) Pd 3d; (c) Ce 3d; (d) Al 2p.

**Table 2**
Atomic ratios obtained by XPS technique of reduced $Al_2O_3$-supported Pd-based catalysts.

| Catalyst | O/Al | Ce/Al ( $\times 10^{-3}$) | Pd/Al ( $\times 10^{-3}$) | Ni/Pd |
|---|---|---|---|---|
| PdCC | 0.97 | | 1.09 | |
| NiPdCe | 1.15 | 3.99 | 1.98 | 0.83 |

Brønsted and Lewis acid sites. $NH_3$-TPD profiles and the amount of $NH_3$ desorbed for both unreduced catalysts are shown in Fig. 5(a) and (b), respectively. The amount of $NH_3$ desorbed is expressed as μmol of $NH_3$ desorbed per gram of catalyst in two zones: (a) low-temperature (LT) peaks (Region I: between 40 and 300 °C) and, (b) high-temperature (HT) peaks (Region II between 300 and 500 °C).

$NH_3$-TPD profiles show three desorption signals. The PdCC catalyst exhibits two LT peaks at about 117 and 205 °C and an HT peak centered at 394 °C, while the NiPdCe catalyst shows that the three desorption peaks were shifted toward higher temperatures, at 158, 208 and 429 °C (Fig. 5(a)). The areas of the NiPdCe signals reveal higher amounts of $NH_3$ desorbed for both Zones I and II (Fig. 5(b)). The ammonia desorption temperatures reflect their acid sites strength and the ammonia desorbed amount is taken as a measurement of the number of acids centres. $NH_3$-TPD results indicate that the NiPdCe catalyst presented both higher strength and number of acid sites compared with the PdCC catalyst. It has been previously demonstrated that the Ni[15] and $CeO_2$[19] incorporation increase the strength of the acid sites in the $Pd/Al_2O_3$ catalysts. Furthermore, the acidity also drastically decreased as the amount of more crystalline $Al_2O_3$ increased, i.e., γ-$Al_2O_3$ (NiPdCe catalyst) presents a higher amount of acid sites compared with δ-$Al_2O_3$ (PdCC catalyst),[29] but it must be considered that the more crystalline phases generally present smaller surface areas, which also would account for the diminished adsorption of ammonia.

### 3.2. Catalytic tests

Before catalytic analysis, it is convenient to mention the reactions that could occur during 1-butyne hydrogenation. It is well-known that hydroisomerization and total hydrogenation reactions are possible when Pd is used as an active component for olefins hydrogenation. Some time ago, Boitiaux et al.[30–32] published a series of articles on liquid-phase hydrogenation of several unsaturated hydrocarbons, such as 1-butene, 1,3-butadiene, and 1-butyne, using supported Pd-, Pt- and Rh-based catalysts. These authors detected the formation of 1-butene, 2-butenes (cis-2-butene and trans-2-butene), and butane during 1-butyne hydrogenation (see Electronic Supplementary Information, ESI, Scheme S2). The amounts of products depend on the hydrogenating and hydroisomerizing capabilities of the catalyst. In this study, the catalytic performances of both reduced $Al_2O_3$-supported Pd-based catalysts were evaluated under the same experimental conditions: temperature, total pressure, and agitation speed of 44 °C, 700 kPa and 2000 r/min, respectively.

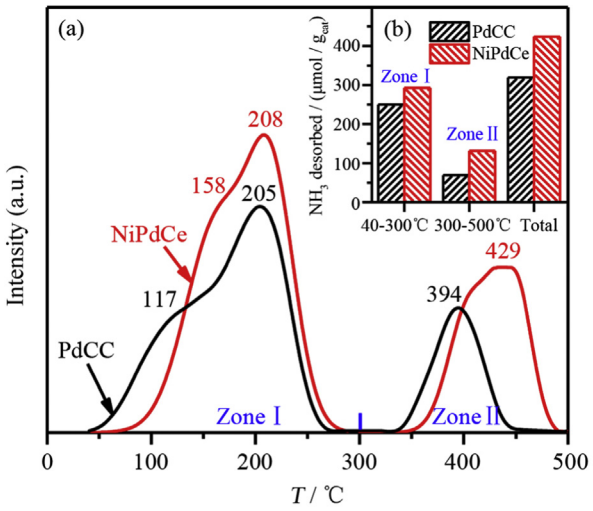


**Fig. 5.** $NH_3$-TPD profiles (a) and acid sites amount (b) of unreduced $Al_2O_3$-supported Pd-based catalysts.

Table 3 shows the 1-butyne conversion during liquid-phase hydrogenation. It can be observed that 1-butyne conversions of both catalysts are similar. At short reaction time, there is a considerable 1-butyne fraction decrease, which is hydrogenated forming only 1-butene. The absence of total hydrogenation (butane) or hydroisomerization products (cis-2-butene and trans-2-butene) at 50% 1-butyne conversion could indicate an inhibition of the 1-butene adsorption due to the higher adsorption strength of 1-butyne. At high reaction time, when 1-butyne concentration decreases, the secondary reactions become much more important. The 1-butyne level from which the catalytic performance starts to behave differently will be named $x^*_{BY}$ and analysed later. First, the selectivity parameters should be defined. The selectivity to the 1-butene formation ($S_{BE}$) as a function of 1-butyne concentration (ppm) is defined by Eq. (1):

$$S_{BE} = \frac{x_{BE} - x^0_{BE}}{x^0_{BY} - x_{BY}} \quad (1)$$

where $x^0_{BE}$ *and* $x^0_{BY}$ are initial molar fractions of 1-butene (BE) and 1-butyne (BY), respectively. The initial molar fraction of BE ($x^0_{BE}$) was zero in all tests. $x_{BE}$ *and* $x_{BY}$ are the corresponding molar fractions of BE and BY at different BY conversions.

Another parameter, also as a function of 1-butyne concentration (ppm), is defined as $S_{H/I}$ (Eq. (2)). The $S_{H/I}$ factor represents the 1-butene fraction that is hydrogenated (butane) regarding the one hydroisomerized (cis-2-butene and trans-2-butene), i.e., the ratio of hydrogenating and hydroisomerization capabilities of the studied catalysts.

$$S_{H/I} = \frac{(x_{BA} - x^{max}_{BA})}{(x_{cBE} - x^{max}_{cBE}) + (x_{tBE} - x^{max}_{tBE})} \quad (2)$$

where $x_{BA}$, $x_{cBE}$ and $x_{tBE}$ are molar fractions of butane (BA), *cis*-2-butene (cBE) and *trans*-2-butene (tBE) at different 1-butyne (BY) conversions. $x^{max}_{BA}$, $x^{max}_{cBE}$ and $x^{max}_{tBE}$ are molar fractions of BA, cBE and tBE when the 1-butene (BE) concentration reaches its highest value.

A previous study, using the same reaction conditions, revealed that the PdCC catalyst is highly selective to 1-butene, as long as the 1-butyne is present inside the catalyst.[5] However, even at high concentrations, the 1-butyne can be depleted from the catalyst due to strong diffusional restrictions. Furthermore, considering that the diffusion of 1-butyne is lower than that of hydrogen, there will be a region into the active shell where the 1-butyne concentration will be essentially zero, allowing the 1-butene adsorption and their

**Table 3**
Conversion at different reaction time of reduced $Al_2O_3$-supported Pd-based catalysts during the 1-butyne hydrogenation.

| Catalyst | 30 min | 60 min | 90 min | 120 min |
|---|---|---|---|---|
| PdCC | 18% | 43% | 76% | 100% |
| NiPdCe | 19% | 49% | 67% | 100% |

subsequent secondary reactions. For concentrations of 1-butyne lower than the value calculated by Eq. (3), $H_2$ exists in excess inside the active region of the catalyst:

$$x^{*}_{BY} = x^{dis}_{H_2}\left(\frac{D_{H_2}}{D_{BY}}\right) \quad (3)$$

where $D_{H_2}$ and $D_{BY}$ are the effective diffusivities of $H_2$ and 1-butyne (BY). $x^{dis}_{H_2}$ is the $H_2$ molar fraction in the solution.

The $x^{dis}_{H_2}$ value is constant because the reaction tests were carried out under the same hydrogen partial pressure. At the used $H_2$ partial pressure, $x^{dis}_{H_2} = 5 \times 10^{-3}$ and, knowing that the diffusivities ratio $(D_{H_2}/D_{BY})$ is about 4, the $x^{*}_{BY}$ value is 16643 ppm, which is represented by the dashed vertical line in Fig. 6.

The most selective catalyst to 1-butene formation will be that which presents the highest $S_{BE}$ value for a given 1-butyne concentration. In this sense, the reduced catalysts present similar $S_{BE}$ values at both high and low 1-butyne concentrations, being $S_{BE} = 1$ at $X_{BY} > x^{*}_{BY}$ (see Fig. 6). On the other hand, it is also observed that when the 1-butyne is being depleted, the secondary reactions become more important. The PdCC catalyst presents higher $S_{H/I}$ value at the same 1-butyne concentrations, i.e., the commercial catalyst presents lower hydroisomerization product concentrations and higher hydrogenation product contents. On the contrary, the NiPdCe catalyst presents a higher hydroisomerization capability and lower hydrogenation when compared with PdCC. The apparent rates of hydrogenation ($r_H$) and hydroisomerization ($r_I$) reactions, obtained at $0.055 > x_{BE} > 0.015$, confirm this statement (see Table 4). Therefore, even though the 1-butyne conversion and selectivity to 1-butene formation are similar, the hydrogenation and hydroisomerization capabilities are different.

The Ni[15] and $CeO_2$[19] incorporation to the $Pd/Al_2O_3$ catalyst has demonstrated improvements in the activity and selectivity in the 1,3-butadiene hydrogenation in the presence of 1-butene under liquid-phase conditions, i.e., the butane formation was suppressed, while the 1-butene recovery was increased. These enhancements were associated with a dilution effect of the Pd-atoms caused by Ni-Pd alloy formation[15] and the acidity characteristics[19] when the Ni and $CeO_2$ were incorporated, respectively. However, the selectivities toward the isomerization products were not previously analyzed.

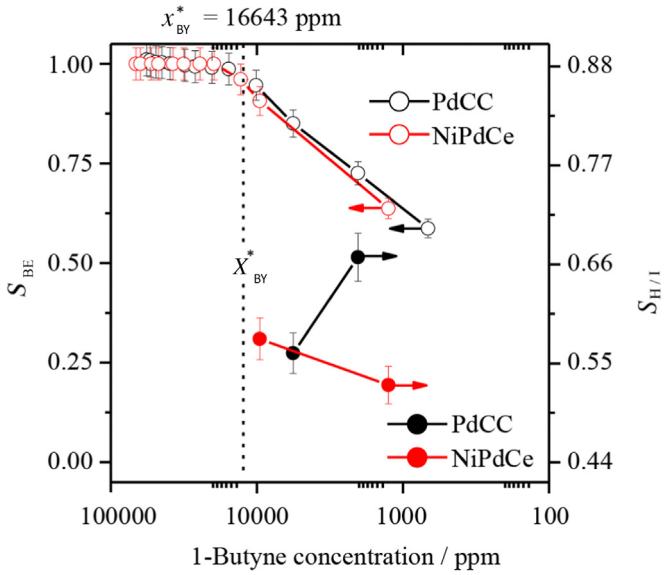


**Fig. 6.** Selectivity to butene formation ($S_{BE}$ factor) and hydrogenation/hydroisomerization ratio ($S_{H/I}$ factor) obtained during the 1-butyne hydrogenation under liquid-phase conditions of reduced $Al_2O_3$-supported Pd-based catalysts.

**Table 4**
Hydrogenation and hydroisomerization reaction rates and hydrogenation/hydroisomerization ratio obtained during the 1-butyne hydrogenation under liquid-phase conditions of reduced $Al_2O_3$-supported Pd-based catalysts.

| Catalyst | $r_H$ ( $\times 10^{-5}$ min$^{-1}$) | $r_I$ ( $\times 10^{-5}$ min$^{-1}$) | $r_H/r_I$ ratio |
|---|---|---|---|
| PdCC | 36.2 | 50.0 | 0.72 |
| NiPdCe | 40.5 | 96.8 | 0.42 |

Hydrogenation rate ($r_H$) and hydroisomerization rate ($r_I$) obtained at $0.055 > x_{BE} > 0.015$.

The hydrogenation and hydroisomerization capabilities observed here could also be associated with those previously studied characteristics (Pd-sites dilution and acidic characteristics),[15,19] but the intrinsic features of the $Al_2O_3$ phase and the electronic properties cannot be discarded. From the XPS results, it is shown that the PdCC catalyst did not show any shift of binding energy values ($Pd_3d$ spectra, Fig. 4(b)) indicating that the second unidentified metal decorates the Pd-surface. On the contrary, in the PdNiCe catalyst, the Pd and Ni atoms formed a bimetallic Pd-Ni nanostructure, suggesting that the electronic density of Pd atoms is changed by Ni incorporation. The higher acidity of the NiPdCe catalyst could also stimulate the hydroisomerization reactions because it is well-known that the 1-butene skeletal isomerization is an acid-catalysed reaction that proceeds via carbenium ion intermediates formed upon protonation of the double bond.

The observed performance could be interesting for some petrochemical processes and might provide a guideline for the development of a Pd-based catalyst with specific catalytic properties. The usefulness of these catalysts opens new avenues for the valorisation of the reaction products to provide novel platform chemicals. Both catalysts could be used for selective hydrogenation of highly unsaturated hydrocarbons because the isomerization and total-hydrogenation products did not begin to appear until the 1-butyne concentration was at least 16643 ppm, suggesting that the preferential adsorption of 1-butyne led to the high selectivity. Additionally, the hydroisomerization products are also of special interest in the $C_4$ HF alkylation pre-treatment or for olefin polymerization pre-treatment because these reactions should proceed without loss of total olefins through over-hydrogenation to alkanes.

## 4. Conclusions

It is demonstrated that both *egg-shell* Pd-based catalysts are highly active and selective toward 1-butene. Furthermore, it is observed that the bifunctional *egg-shell* $NiPd/CeO_2–Al_2O_3$ catalyst presents a higher capability toward the hydroisomerization reactions, while the egg-shell promoted $Pd/Al_2O_3$ commercial catalyst exhibits higher hydrogenating capability. It is suggested that in the commercial catalyst the Pd-atoms are decorated by a second metal (unidentified), while a bimetallic Pd–Ni nanostructure is formed in the lab-prepared catalyst, which can be responsible for their observed catalytic behaviour. The higher hydroisomerization rate in the NiPdCe catalyst can be associated with its stronger surface acidity due to the more acidic $\gamma$-$Al_2O_3$ phase in the support and the $CeO_2$ incorporation.

## Acknowledgements

The authors would like to acknowledge the technical assistance of Yraida Diaz (IVIC, $N_2$ physisorption), Edgar Cañizales (INTEVEP, HRTEM) and Omar Ocando (INTEVEP, XPS).

## Appendix A. Supplementary data

Supplementary data to this article can be found online at https://doi.org/10.1016/j.jre.2020.09.017.

## References


1. Alves JA, Bressa SP, Martínez OM, Barreto GF. Kinetic study of the liquid-phase selective hydrogenation of 1-butyne in presence of 1-butene over a commercial palladium-based catalyst. *Chem Eng Res Des*. 2011;89:384.
2. Derrien ML. Selective hydrogenation applied to the refining of petrochemical raw materials produced by steam cracking. *Stud Surf Sci Catal*. 1986;27:613.
3. Ardiaca NO, Bressa SP, Alves JA, Martínez OM, Barreto GF. Experimental procedure for kinetic studies on egg-shell catalysts: the case of liquid-phase hydrogenation of 1,3-butadiene and n-butenes on commercial Pd catalysts. *Catal Today*. 2001;64:205.
4. Alves JA, Bressa SP, Martínez OM, Barreto GF. Kinetic study of the selective catalytic hydrogenation of 1,3-butadiene in a mixture of n-butenes. *J Ind Eng Chem*. 2012;18:1353.
5. Alves JA, Bressa SP, Martínez OM, Barreto GF. Kinetic evaluation of the set of reactions in the selective hydrogenation of 1-butyne and 1,3-butadiene in presence of n-butenes. *Ind Eng Chem Res*. 2013;52:5849.
6. García-Colli G, Alves JA, Martínez OM, Barreto GF. Development of a multi-layer microreactor: application to the selective hydrogenation of 1-butyne. *Chem Eng Process*. 2016;105:38.
7. Zhang LL, Zhou MX, Wang AQ, Zhang T. Selective hydrogenation over supported metal catalysts: from nanoparticles to single atoms. *Chem Rev*. 2020;120:683.
8. Delage M, Didillon B, Huiban Y, Lynch J, Uzio D. Highly dispersed Pd based catalysts for selective hydrogenation reactions. *Stud Surf Sci Catal*. 2000;130:1019.
9. Méndez FJ, Villasana Y, Guerra J, Sifontes AB, Olivera-Fuentes C, Brito JL. Aspectos relevantes de la hidrogenación selective de 1,3-butadieno con catalizadores basados en $Pd/Al_2O_3$. *Catálisis*. 2012;1:48.
10. Renouprez A, Faudon JF, Massardier J, Rousset JL, Delichère P, Bergeret G. Properties of supported Pd-Ni catalysts prepared by coexchange and organometallic chemistry. Part II: correlation between the reactivity for butadiene hydrogenation and the surface properties studied by XPS and LEIS. *J Catal*. 1997;170:181.
11. Sárkány A. Promoting effect of Ni in semi-hydrogenation of 1,3-butadiene over Ni-Pd catalysts. *Stud Surf Sci Catal*. 2000;130:2081.
12. Saint-Lager MC, Jugnet Y, Dolle P, Piccolo L, Baudoing-Savois R, Bertolini JC, et al. $Pd_8Ni_{92}(100)$ surface structure from surface X-ray diffraction: surface evolution under hydrogen and butadiene reactants at elevated pressure. *Surf Sci*. 2005;587:229.
13. Massard R, Uzio D, Thomazeau C, Pichon C, Rousset JL, Bertolini JC. Strained Pd overlayers on Ni nanoparticles supported on alumina and catalytic activity for buta-1,3-diene selective hydrogenation. *J Catal*. 2007;245:133.
14. Hou RJ, Yu WT, Porosoff MD, Chen JG, Wang TF. Selective hydrogenation of 1,3-butadiene on PdNi bimetallic catalyst: from model surfaces to supported catalysts. *J Catal*. 2014;316:1.
15. Méndez FJ, Solano R, Villasana Y, Guerra J, Curbelo S, Inojosa M, et al. Selective hydrogenation of 1,3-butadiene in presence of 1-butene under liquid phase conditions with $NiPd/Al_2O_3$ catalysts. *Appl Petrochem Res*. 2016;6:379.
16. Hou ZQ, Pei WB, Zhang X, Zhang KF, Liu YX, Deng JG, et al. Rare earth oxides and their supported noble metals in application of environmental catalysis. *J Rare Earths*. 2020;38:819.
17. Lozano L, Guerra J, Curbelo S, Brito JL, Olivera-Fuentes C. Synthesis and characterization of $NiPdCe/\gamma\text{-}Al_2O_3$ catalyst for selective hydrogenation of 1,3-butadiene: impregnation conditions study. *Chem Engineer Trans*. 2011;24:55.
18. Lozano L, Brito JL, Olivera C, Guerra J, Curbelo S. Influence of toluene on the catalytic activity of NiPdCe catalyst for selective hydrogenation of 1,3-butadiene. *Fuel*. 2013;110:76.
19. Méndez FJ, Piccolo L, Solano R, Aouine M, Villasana Y, Guerra J, et al. Promoting effect of ceria on the performance of $NiPd/(CeO_2\text{-})Al_2O_3$ catalysts for the selective hydrogenation of 1,3-butadiene in presence of 1-butene. *New J Chem*. 2018;42:11165.
20. Méndez FJ, Sanz O, Montes M, Guerra J, Olivera-Fuentes C, Curbelo S, et al. Selective hydrogenation of 1,3-butadiene in the presence of 1-butene under liquid phase conditions using structured catalysts. *Catal Today*. 2017;289:151.
21. Alves JA, Bressa SP, Martínez OM, Barreto GF. Kinetic study of the liquid-phase hydrogenation of 1-butyne over a commercial palladium/alumina catalyst. *Chem Eng J*. 2007;125:131.
22. Moulder JF, Stickle WF, Sobol PE, Bomben KD. *Handbook of X-ray photoelectron spectroscopy*. 2nd ed. Minnesota, MN: Perkin-Elmer Corporation; 1992.
23. Hillebrecht FU, Fuggle JC, Bennett PA, Zołnierek Z, Freiburg C. Electronic structure of Ni and Pd alloys Part II: X-ray photoelectron core-level spectra. *Phys Rev B: Condens Matter*. 1983;27:2179.
24. Bèche E, Charvin P, Perarnau D, Abanades S, Flamant G. Ce 3d XPS investigation of cerium oxides and mixed cerium oxide ($Ce_xTi_yO_z$). *Surf Interface Anal*. 2008;40:264.
25. Paparazzo E. On the curve-fitting of XPS Ce(3d) spectra of cerium oxides. *Mater Res Bull*. 2011;46:323.
26. Deshpande S, Patil S, Kuchibhatla SV, Seal S. Size dependency variation in lattice parameter and valency states in nanocrystalline cerium oxide. *Appl Phys Lett*. 2005;87:133113.
27. Chen M, Wang X, Yu YH, Pei ZL, Bai XD, Sun C, et al. X-ray photoelectron spectroscopy and Auger electron spectroscopy studies of Al-doped ZnO films. *Appl Surf Sci*. 2000;158:134.
28. Yang YF, Jin YZ, He HP, Ye ZZ. Facile synthesis and characterization of ultrathin cerium oxide nanorods. *CrystEngComm*. 2010;12:2663.
29. Pattamakomsan K, Suriye K, Dokjampa S, Mongkolsiri N, Praserthdam P, Panpranot J. Effect of mixed $Al_2O_3$ structure between $\theta$- and $\alpha\text{-}Al_2O_3$ on the properties of $Pd/Al_2O_3$ in the selective hydrogenation of 1,3-butadiene. *Catal Commun*. 2010;11:311.
30. Boitiaux JP, Cosyns J, Robert E. Liquid phase hydrogenation of unsaturated hydrocarbons on palladium, platinum and rhodium catalysts. Part I: kinetic study of 1-butene, 1,3-butadiene and 1-butyne hydrogenation on platinum. *Appl Catal*. 1987;32:145.
31. Boitiaux JP, Cosyns J, Robert E. Liquid phase hydrogenation of unsaturated hydrocarbons on palladium, platinum and rhodium catalysts. Part II: kinetic study of 1-butene, 1,3-butadiene and 1-butyne hydrogenation on rhodium; comparison with platinum and palladium. *Appl Catal*. 1987;32:169.
32. Boitiaux JP, Cosyns J, Robert E. Hydrogenation of unsaturated hydrocarbons in liquid phase on palladium, platinum and rhodium catalysts. Part III: quantitative selectivity ranking of platinum, palladium and rhodium in the hydrogenation of 1-butene, 1,3-butadiene and 1-butyne using a single reaction scheme. *Appl Catal*. 1987;35:193.